https://doi.org/10.1016/j.engstruct.2020.110669

Experimental and numerical investigation on stub column behaviour of cold-formed octagonal hollow sections

Junbo Chen[1,2], Jiong-Yi Zhu[1,2], Tak-Ming Chan[1,2]*

[1]Department of Civil and Environmental Engineering, The Hong Kong Polytechnic University, Hung Hom, Hong Kong, China
[2]Chinese National Engineering Research Centre for Steel Construction (Hong Kong Branch), The Hong Kong Polytechnic University, Hung Hom, Hong Kong, China
*Corresponding author: tak-ming.chan@polyu.edu.hk

Abstract: This paper presents an experimental and numerical investigation into stub column behaviour of cold-formed steel octagonal hollow sections (OctHSs). A total of 16 OctHS stub columns were tested. Tensile coupons were extracted from both flat and corner portions of hollow sections to determine corresponding material properties. Finite element (FE) models were developed using commercially available software ABAQUS to replicate the test results generated in this study. The degree to which the enhanced material properties at corners should be extended was investigated. It was found that FE models with corner material properties extended to a width of material thickness beyond the corner portions offer the best agreement with test observations. The validated FE models were then adopted to conduct parametric studies to supplement test database. Cross-sectional slenderness limits specified in current design codes, including EN 1993-1-1, ANSI/AISC 360-16, ASCE/SEI 48-11 and AISI S100-16 (DSM) were evaluated against the test results in conjunction with the FE results. It was found that current limits are not suitable for the design of OctHSs. New cross-sectional slenderness limits in accordance with EN 1993-1-1, ANSI/AISC 360-16, ASCE/SEI 48-11 and DSM were then proposed based on the test and FE results. Cross-sectional capacity predictions obtained from EN 1993-1-1, ANSI/AISC 360-16, ASCE/SEI 48-11 and DSM were also compared with test and FE results. It is shown that the capacity predictions for slender sections from ASCE/SEI 48-11 are slightly unsafe, and ANSI/AISC 360-16 produces relatively satisfactory capacity predictions.

Keywords: Stub column; Cold-formed section; OctHS; FEM; Design.

1. Introduction

High strength steels with a nominal yield strength higher than 460 MPa have been commercially available and widely adopted in civil structural applications owing to their structural efficiency such as high strength-to-weight ratio, cost efficiency and low carbon footprint [1]. Since steel hollow sections have been increasingly used in structures [2], numerous experimental and numerical investigations in steel hollow sections focusing on high strength steel have been carried out. Behaviours of steel hollow sections with square, rectangular and circular cross-sections have been extensively studied at material properties level [1, 3], cross-sectional level [3-7] and member level [8].

In recent years, polygonal steel hollow sections, in particular octagonal hollow sections (OctHSs), have attracted significant interests from structural engineers and architects and have been employed in civil applications such as transmission poles, telegraph towers and lattice structures [9, 10]. An example of OctHS lighting column is depicted in Fig. 1. An obvious attraction of OctHSs is that the flat side width is smaller than square or rectangular counterparts provided that they have the same perimeter. OctHSs therefore exhibit stronger local buckling resistances than that of square/rectangular hollow sections (SHSs/RHSs) [10, 11]. In addition, OctHSs have flat surfaces, providing easier beam-to-column connection constructions as compared with circular hollow sections (CHSs) [10, 11]. Design rules for OctHSs have been specified in an ASCE standard for steel transmission pole structures ASCE/SEI 48-11 [12]. However, design of OctHSs is not included in any currently used structural steel design specifications like EN 1993-1-1 [13], EN 1993-1-12 (supplementary rules to EN 1993-1-1 for high strength steel) [14] and ANSI/AISC 360-16 [15]. To date, experimental research on material properties and residual stresses of OctHSs could be found in S355 steel [16], Q460 steel [11] and S690 steel [10]. However, studies on structural behaviours of OctHSs made from high strength steel remain limited. Aoki et al. [17] experimentally investigated the compressive cross-sectional capacity of OctHSs through 6 stub column tests. Steel plates used in this study had a yield strength of 289 MPa. Compressive cross-sectional strengths of OctHSs were also investigated by Mitiga et al. [18] and Migita and Fukumoto [19]. Yield strengths of the steel plates employed in [18, 19] were 289 MPa and 307 MPa. Godat et al. [20] tested 2 OctHS stub column specimens and the yield strength of the steel plates is 265 MPa and 279 MPa. A stub column test on OctHS with measured yield strength of 296 MPa was found in Zhu and Chan [21]. Both experimental and numerical studies on OctHSs using S355 steel (the measured yield strength was 379 MPa) were conducted by Zhu et al. [16]. Han et al. [22] carried out a test programme consisting of 18 stub column specimens fabricated using S690 steel. It can be concluded that studies using high strength steel with yield strengths ranging from 460 MPa to 690 MPa are extremely limited, potentially inhibiting attempts to develop effective design recommendations for OctHSs.

Therefore, an experimental and numerical investigation on cold-formed OctHSs using Q460 steel (with a nominal yield strength of 460 MPa) was undertaken herein to advance the design of OctHSs. Two batches of Q460 steel with nominal thickness of 3 mm and 6 mm were used. A total of 16 OctHS stub column tests were conducted. Tensile coupons were extracted from both flat and corner portions of the hollow sections to determine corresponding material properties. Subsequently, finite element (FE) models were developed and validated by the generated test results. The validated FEs were then adopted to carry out parametric studies to provide supplementary data. The experimental and numerical results were used together to evaluate the current design methods.

2. Experimental investigations

To form an OctHS, there are three general fabrication routes as discussed in [10, 11]: (1) welding eight flat plates (built-up section), (2) welding two cold-formed half-sections at two corners (cold-formed section), and (3) welding two cold-formed half-sections at two flat surfaces (cold-formed section). The cold-formed half-sections were manufactured from steel plates by press-braking. This study only focused on cold-formed sections. Therefore, fabrication routes (2) and (3), denoted as CF1 and CF2, respectively, were employed as shown in Fig. 2. The former cold-formed half-section has three cold-bent corners, while the latter has four cold-bent corners. Another main difference between these two fabrication routes was the location of the welding seams. Two batches of steel plates with nominal thicknesses of 3 mm and 6 mm were employed in the study. The measured yield strengths of parent metals of 3 mm and 6 mm steel are 546.5 MPa and 580.7 MPa, respectively. The steel plates for each thickness were produced in the same batch for a direct comparison.

2.1 Specimens

A total of 16 cold-formed octagonal hollow section specimens were included in this test. A specimen label system is used throughout this study, which firstly specifies the cross-sectional shapes of the specimen: O for OctHSs. Following the cross-sectional shape, cross-sectional dimensions are given by $B\times t$. Fabrication routes are finally given after a hyphen. The definitions of symbols for OctHSs are demonstrated in Fig. 2, where H is the overall width of an OctHS, B is the side width of an OctHS, b is the clear width of a flat side excluding corner portions, t is the thickness of material, and r_o and r_i are the outer and inner corner radii of the cross-section. For example, the label "OC75×6-CF1" designates an OctHS specimen manufactured by route CF1 with nominal side width and thickness of 75 and 6 mm, respectively.

The measured dimensions of OctHSs are reported in Table 1. The symbol # in the suffix indicates a repeated test to assess the accuracy and repeatability of the experimental tests. The length L of OctHS specimens is equal to $3H$ to ensure that all the specimens are stub columns. It can be seen that wide ranges of parameters were covered. The side width B of the OctHSs ranges from 60.8 mm to 106.8 mm and the thickness t varies from 3.03 mm to 5.83 mm, resulting in a b/t ratio ranging from 10.3 to 32.3.

For a regular OctHS, the relation between the side width B and the overall depth H is formulated by Eq. (1). The mid-surface flat width b_p of OctHSs is determined from Eq. (2), where h_p is the overall width of the mid-surface and t is the thickness of the tube.

$$B=H/\left(1+\sqrt{2}\right) \tag{1}$$

$$b_p=h_p/\left(1+\sqrt{2}\right)=\left(H-t\right)/\left(1+\sqrt{2}\right) \tag{2}$$

The clear width of a flat side excluding corner portions b can be obtained by Eq. (3):

$$b = B\text{-}2r_o \cdot \tan\theta \tag{3}$$

in which θ is the interior angle of OctHSs, equal to π/8, and r_o is the outer corner radius. The cross-sectional area A of OctHSs was calculated from Eq. (4), where r_i is the inner corner radius.

$$A = 8 \times b \times t + \pi\left(r_o^2 - r_i^2\right) \tag{4}$$

2.2 Material properties

A series of tensile coupon tests were carried out to determine material properties. Tensile coupons were extracted from both flat and corner portions of the hollow sections. The tensile coupon tests were conducted using a 500 kN Instron testing system in accordance with EN ISO 6892-1:2016 [23]. Strain gauges were affixed to obtain elastic modulus and to determine stress-strain curves at the initial stage. An extensometer was used to record full stress-strain curves up to fracture. During each tensile coupon test, the loading was paused twice near yield and ultimate strength for 120 seconds to allow for stress relaxation to obtain the static stress-strain curves [24]. The obtained static stress-strain curves were then used to determine the static material properties, such as yield strength and ultimate strength.

Material properties of parent metals were firstly obtained through flat coupon tests. Mean measured properties are summarised in Table 2, in which E_s is the elastic modulus of steel, v is the Poisson's ratio, f_y is the yield strength, f_u is the ultimate strength, ε_u is the strain at the ultimate strength, ε_{sh} is the strain-hardening strain at which strain-hardening initiates and ε_f is the proportional elongation at fracture. The yield strengths of the 3 mm and 6 mm steel plates are 546.5 MPa and 580.7 MPa, respectively. Typical full stress-strain curves of parent metals are depicted in Fig. 3.

Material properties at flat and corner portions of the specimens were determined via flat and corner coupon tests. Test results of the tensile coupons extracted from OctHSs could be found in [11]. Mean measured material properties of flat and corner portions extracted from [11] are summarised in Tables 3 and 4, where E_s is the elastic modulus, f_y is the yield strength (taken as lower yield strength for steel with yield plateau or 0.2% proof strength for steel exhibiting rounded stress-strain relationship), f_u is the ultimate strength, ε_u is the strain at ultimate strength, and ε_f is the proportional elongation at fracture. The letters "f" and "c" in the subscript designate flat and corner coupons extracted from hollow tubes, respectively. Typical stress-strain curves of material from flat and corner portions are presented in Fig. 4.

By comparing the material properties of corner coupons to that of flat coupons, it was observed that cold-forming process produces essentially unchanged properties at the flat regions but causes large strength enhancements at the corners as a result of excessive strain-hardening [25]. The yield strength at corner over the yield strength at flat region ratios $f_{y,c}$ / $f_{y,f}$, also termed as strength enhancement ratio, are 1.21 and 1.27 in OctHSs for the 3 mm and 6 mm steels, respectively.

2.3 Geometric imperfection

Prior to the execution of the stub column tests, initial local geometric imperfection for all the OctHS specimens was measured on a milling machine. Three linear variable displacement transducers (LVDTs) were used to measure the imperfection in each surface of the specimen, as shown in Fig. 5. The magnitude of the out-of-flatness at the central lines could be then calculated by $[(\Delta_{c1}+\Delta_{c2})/2]-\Delta_m$, where Δ_{c1}, Δ_{c2} and Δ_m are readings recorded from LVDTs c1, c2 and m, as shown in Fig. 5. The measurements were started and terminated at the location 50 mm away from each end of the specimens to eliminate the possible local imperfection caused by cold sawing [4]. The same configuration of imperfection measurements has been adopted in similar studies like Ma et al. [4] and Zhu et al. [16]. The measured maximum amplitudes of local geometric imperfection (ω_0) for each specimen are reported in Table 1.

2.4 Stub column tests

The stub column tests were prepared and tested at The Hong Kong Polytechnic University. All specimens had both ends milled flat and square before testing. Therefore, the end surfaces and the parallel plates of the compression machine contacts well, and a uniform compressive load was ensured. Two steel rings with a height of 20 mm were used to strengthen the end surfaces to avoid premature end failures. All the stub column specimens were compressed at a constant loading speed of 0.05%L mm/min, which is equivalent to the initial strain rate for tensile coupon tests. Similar to tensile coupon tests, the stub column tests were paused for 120 seconds near the ultimate load to allow for stress relaxation. The static axial load versus end shortening were then obtained.

Strain gauges were mounted at the mid-height of the specimens and four linear variable displacement transducers (LVDTs) were located between two parallel end-plates of the testing machine to record the end shortening of the stub columns. The arrangements of the strain gauges and LVDTs and the test set-up are shown in Fig. 6. Special steel rings were clamped to the specimens near the ends in order to prevent premature failures at the ends, as suggested by [4, 16]. End shortening was obtained by combining the strain gauge data with the LVDT readings. Strain gauges readings were used to modify the initial stage of LVDT readings, which removes the effects of initial gaps and end platen deformation, thereby giving true specimen end shortening [26]. Key experimental results of the OctHS stub column tests, including the ultimate axial load N_u, the end shortening at ultimate load δ_u, yield load N_y and the ultimate-to-yield load ratio N_u/N_y are summarised in Table 5. The yield load N_y is obtained by $A \times f_{y,cs}$, in which $f_{y,cs}$ is the average yield strength of cold-formed hollow sections weighted by the area of flat regions and corner regions. Full sets of static axial load-end shortening responses recorded from the OctHS stub column tests are depicted in Fig. 7. It was also observed that the two fabrication routes produced similar test results, indicating that fabrication routes discussed in this study have negligible effect on the stub column test in terms of ultimate load and axial load-end shortening curves. With regards to failure modes, all the stub columns failed by either elephant foot buckling or local buckling whereby the faces of the cross sections locally buckled alternately outwards and inwards.

3. Numerical simulations

3.1 Finite element modelling

In parallel with the experimental tests, numerical simulations by means of finite element (FE) modelling were carried out using commercially available finite element software package ABAQUS [27]. Primary aims of the numerical analyses were firstly to replicate the test observations, and subsequently to conduct parametric studies using the validated FE models to supplement the generated test results to investigate the effects of key parameters.

The element type chosen for numerical analyses is four-node shell element with reduced integration, S4R, which has been extensively used to predict the structural responses of steel hollow sections in previous studies [4, 5, 7, 8, 21, 28]. For each stub column test, the whole cross-section was modelled with the measured geometries. With regards to boundary conditions, both ends of the stub columns were fully restrained against all degrees of freedom except for the axial translation at the loaded end. The axial load was applied by displacement increments using the "Static, general" function available in ABAQUS. Mesh convergence studies were conducted to determine a suitable mesh size for analyses. The mesh sensitivity study shows that a mesh size of $B/10$ for OctHSs yields suitably accurate predictions while maximizing computational efficiency at the same time, where B is the side width of the OctHSs. The mean measured material properties were used in FE models. The input material behaviour is specified in terms of true stress and log plastic strain. The true stress and log plastic strain were converted from engineering stress-strain curves obtained from the coupon tests taken from hollow sections. In the FE models, strength enhancement at corners is allowed for by assigning the corner material properties to corner portions and to extended corner regions. In cold-formed SHSs/RHSs, extended corner regions with a width of $2t$ are commonly used, where t is the material thickness [4, 5, 7, 8]. However, in cold-formed OctHSs, the bend angle is 45°, which is only half of that of SHS/RHSs. Therefore, the influence of the cold-forming process may be different and the degree to which the enhanced corner properties should be extended beyond the curved corner portions for OctHSs is still unclear. A parametric study was therefore conducted herein to investigate the behaviour of OctHS stub columns with or without enhanced strength regions. Four cases were considered: (1) corner strength enhancement was not considered; (2) enhanced corner material properties was assigned to curved corner portions only; (3) enhanced strength regions were extended to a width of t beyond the curved corner portions; and (4) enhanced strength regions were extended to a width of $2t$ beyond the curved corner portions, as shown in Fig. 8. The lowest elastic eigenmode, generated from linear elastic buckling analyses, was taken as the profile of initial geometric imperfection to simulate the distribution of local imperfection, examples of which is shown in Fig. 9. The measured maximum imperfection amplitude ω_0 of each specimen was used.

The effect of residual stresses was also considered in this study. For cold-formed steel members, residual stresses are introduced as a result of fabrication processes. Residual stresses exist in both longitudinal and transverse directions. Longitudinal residual stresses are more influential to stub column behaviours when compared to transverse residual stresses. Longitudinal residual stresses are composed of membrane and bending residual stresses, which are introduced largely due to welding and cold-forming, respectively. The effect of bending residual stresses is to lead to premature material yielding. It was observed from [11] that coupons cut from cold-formed hollow sections curved longitudinally after extraction as a result of bending residual stresses. During the initial stage of coupon tests, the elastic straightening of the curved coupons approximately reintroduced the bending residual stresses [28], demonstrating that the effect of bending residual stress is included in the material properties. Therefore, since material properties were determined from coupons taken from cold-formed hollow sections, the bending residual stresses do not need to be defined in the FE models. Membrane residual stresses were considered, and the predictive models proposed in [11] were explicitly defined in the FE models through the '*Initial condition' command. A typical residual stress distribution incorporated in the FE model for the specimen O75×3-CF2 is presented in Fig. 10. Positive values indicate tensile membrane residual stresses while negative values indicate compressive membrane residual stresses. To investigate the effect of residual stresses, FE models were conducted with and without residual stresses while other parameters remained the same. Fig. 11 displays the axial load versus end shortening curves of specimen O75×3-CF2. The axial load versus end shortening curves of FE models with and without residual stresses are almost identical, only an earlier yielding of the steel tube (reflected by the earlier drop at the post-peak stage) was observed. The existence of residual stresses causes an earlier yielding of the material initially in compression. Residual stresses near welding seams are as high as 55% of steel yield strength [11], however the percentage of area is relatively low. Magnitudes of residual stresses in other regions are comparatively small, thereby leading to a negligible effect on the stub column behaviour in terms of axial load versus end shortening curves. Therefore, in the following study, residual stresses were not incorporated.

3.2 Validation of FE models

The failure mode, ultimate axial load and axial load versus end shortening curves generated by FE models were compared with those obtained from experimental tests to assess the accuracy of the models. Fig. 12 shows the failure modes of OctHS stub columns observed from test results and FE models. The failure modes generated from FE models are shown to closely match the test observations. Comparisons of axial load versus end shortening curves of the stub column tests are presented in Fig. 13. The axial load versus end shortening curves predicted from FE models were found to correlate well with that of test results. Table 5 summarises the ultimate load obtained from FE models and test results. Mean values of FE N_u / Test N_u of the four considered cases (different degrees of the extension of corner properties) for OctHS stub columns are 0.97, 0.99 and 1.00, and 1.01 respectively with corresponding CoVs of 0.02, 0.02, 0.02 and 0.03. Examples of axial load versus end shortening curves from specimen O60×3-CF1 and corresponding FE models of four considered cases are shown in Fig. 14. It was found that FE models with corner properties extended to material thickness t beyond the curved portions of the cross-sections yield the best agreement with test results than others.

It is shown that the predicted ultimate load agrees well with test results. Hence, it is concluded that the developed FE models can produce accurate predictions in terms of failure modes, ultimate axial loads, and axial load versus end shortening curves.

3.3 Parametric study

With the satisfactory ability to replicate test results, the validated FE models were adopted to carry out parametric studies, aiming at generating FE results over a broader range of cross-sectional slenderness to supplement the test results. Two OctHSs tested in this study, O75×6-CF1 and O90×3-CF1, were chosen as the basis of the parametric study. The geometries (excluding the thickness) and measured material properties were used. A local geometric imperfection amplitude of $0.07t$, an outer corner radius of $3t$ and an inner corner radius of $2t$ were adopted based on statistical analyses of the test specimens. Variations in the cross-sectional slenderness were achieved through gradually modifying the material thickness t. A total of 42 FE models were developed in the parametric studies. The results of the parametric studies are used in conjunction with the test results to assess the current design codes for OctHSs under axial compression.

4. Assessment of current design codes

4.1 Current design methods

4.1.1Cross-sectional classification

EN 1993-1-1 [13] and ANSI/AISC 360-16 [15] adopt the concept of cross-section classification and the effective width method for the design of steel hollow sections, including CHSs, SHSs and RHSs. For cross-sections under axial compression, the cross-sections that can reach the yield strength are classified as Class 1-3 or non-slender sections, whilst those with local buckling occurred in the elastic stage before the yield strength are considered as Class 4 or slender sections. Maximum width-to-thickness or diameter-to-thickness ratios, also termed as cross-sectional slenderness limits, are stipulated for compression parts. Slenderness limits specified in EN 1993-1-1 and ANSI/AISC 360-16 for CHSs and SHSs/RHSs are expressed in Eqs. (5-8) respectively (assuming $E_s = 210$ GPa), where D is outer diameter of CHSs, t is material thickness, f_y is the steel yield strength, E is the elastic modulus of steel, and b is the clear width of SHSs/RHSs.

$$D / t \le 90 \times \frac{235}{f_y} \text{ (EN 1993-1-1 for CHS)} \tag{5}$$

$$b / t \le 42\sqrt{\frac{235}{f_y}} \text{ (EN 1993-1-1 for SHS/RHS)} \tag{6}$$

$$D / t \le 0.11 \times \frac{E}{f_y} \approx 98.3 \times \frac{235}{f_y} \text{ (ANSI/AISC 360-16 for CHS)} \tag{7}$$

$$b / t \le 1.4\sqrt{\frac{E}{f_y}} \approx 41.85\sqrt{\frac{235}{f_y}} \text{ (ANSI/AISC 360-16 for SHS/RHS)} \tag{8}$$

It should be noted that limit for OctHSs is not specified in neither EN 1993-1-1 nor ANSI/AISC 360-16. ASCE standard ASCE/SEI 48-11 [15] specifies the cross-section slenderness limit for Class 1-3 SHSs/RHSs, as shown in Eq. (9), and this limit is extended to the design of regular OctHSs.

$$b / t \le 2.62 \times \frac{260}{\sqrt{f_y}} \approx 44.4\sqrt{\frac{235}{f_y}} \tag{9}$$

The direct strength method (DSM), which is currently incorporated in AISI S100-16 [29], was initially proposed for the design of cold-formed sections with flat elements. This method was also considered herein. The DSM utilises an overall cross-section slenderness (λ_p), defined in Eq. (10), to determine the cross-sectional capacity, in which f_y is the steel yield strength, f_{cr} is the elastic buckling stress.

$$\lambda_p = \sqrt{f_y / f_{cr}} \tag{10}$$

Observed from previous study [16], the elastic buckling stress of OctHSs may be determined by steel plate theory as presented in Eq. (11), where E_s is the elastic modulus of steel, v is the Poisson's ratio of steel, b_p is the side width of OctHS middle surface, t is the material thickness, and k is the plate buckling coefficient. The k values for regular polygonal hollow sections have been numerically investigated in previous studies, such as Migita and Fukumoto [19] and Teng et al. [30], and a value of 4 was suggested for OctHSs, which is the same as SHSs/RHSs.

$$f_{cr} = k\frac{\pi^2 E_s}{12(1-v^2)}\left(\frac{t}{b_p}\right)^2 \tag{11}$$

4.1.2 Cross-sectional capacity

The effective width method is commonly adopted in current design codes for the design of sections with slender plate elements. It has been standardised in ANSI/AISC 360-16 [16] and EN 1993-1-5 [31]. The original Winter's effective width formula is $\rho = b_e/b = 1.9(t/b)\sqrt{E_s/f_y}\,[1-0.415(t/b)\sqrt{E_s/f_y}\,] \le 1$, in which ρ is the reduction factor and b_e is the effective width of slender plate elements. The Winter's formula can be simplified as Eq. (12), in which λ_p is the plate slenderness obtained from Eq. (10).

$$\rho = \begin{cases} 1 & \text{for } \lambda_p \le 0.673 \\ \left(1 - 0.22/\lambda_p\right)/\lambda_p & \text{for } \lambda_p > 0.673 \end{cases} \tag{12}$$

The expression of the effective width formula in EN 1993-1-5 [31] is given in Eq. (13), slightly different from Eq. (12), in which ψ is the stress ratio, taken as 1.0 for uniform compression.

$$\rho = \begin{cases} 1 & \text{for } \lambda_p \le 0.5 + \sqrt{0.085 - 0.055\psi} \\ \left(1 - 0.055(3+\psi)/\lambda_p\right)/\lambda_p \le 1.0 & \text{for } \lambda_p > 0.5 + \sqrt{0.085 - 0.055\psi} \end{cases} \tag{13}$$

It should be noted that the design of cross-sectional capacity of OctHSs under axial compression is not included in these codes. ASCE standard ASCE/SEI 48-11 provides a set of design equations for regular OctHSs, as expressed in Eq. (14), where f_y is the steel yield strength, A is the gross cross-sectional area, b is the clear width of a flat side excluding corner portions, and t is the material thickness.

$$N_{\mathrm{ASCE}} = \begin{cases} f_{\mathrm{y}} A & \text{for } b/t \le 2.62 \times \dfrac{260}{\sqrt{f_{\mathrm{y}}}} \\ 1.42 f_{\mathrm{y}} \left(1.0 - 0.00114 \dfrac{\sqrt{f_{\mathrm{y}}}}{2.62} \dfrac{b}{t} \right) A & \text{for } b/t > 2.62 \times \dfrac{260}{\sqrt{f_{\mathrm{y}}}} \end{cases} \tag{14}$$

The DSM nominal compressive capacity of cross-sections subjected to local buckling could be obtained from Eq. (15), in which λ_p is overall cross-section slenderness and can be obtained from Eq. (10).

$$N_{\mathrm{DSM}} = \begin{cases} f_{\mathrm{y}} A & \text{for } \lambda_{\mathrm{p}} \le 0.776 \\ (1 - \dfrac{0.15}{\lambda_{\mathrm{p}}^{0.8}}) \dfrac{1}{\lambda_{\mathrm{p}}^{0.8}} f_{\mathrm{y}} A & \text{for } \lambda_{\mathrm{p}} > 0.776 \end{cases} \tag{15}$$

4.2 Assessment

4.2.1 Cross-sectional classification

As mentioned above, steel plate theory can be used to determine the elastic buckling stress of OctHSs owing to the flat elements within OctHSs. Therefore, the specified limits for SHSs/RHSs in EN 1993-1-1, ANSI/AISC 360-16 and ASCE/SEI 48-11 were evaluated by the test results and FE results generated in this study. It should be noted that the limit in ANSI/AISC 360-16 (converted to $41.85\sqrt{235/f_y}$) is very close to that of EN 1993-1-1 ($42\sqrt{235/f_y}$). It was therefore not included in the assessment. The cross-section slenderness limit specified in the DSM (0.776 in Eq. (15)) was also assessed. The elastic buckling stress of OctHSs was calculated using Eq. (11). Results of cross-sectional slenderness assessments are depicted in Fig. 15. It could be concluded that within the scope of this study the current slenderness limits specified in EN 1993-1-1, ASCE/SEI 48-11 and DSM are not safe for the design of OctHSs. New slenderness limits for plate buckling in OctHSs in accordance with EN 1993-1-1, ANSI/AISC 360-16, ASCE/SEI 48-11 and DSM were proposed (see Eqs. (16-19)) by the regression analysis on the basis of test and FE results as shown in Fig. 15.

$$b/t \le 34.1\sqrt{\frac{235}{f_y}} \text{ (for EN 1993-1-1)} \tag{16}$$

$$b/t \le 1.14\sqrt{\frac{E_s}{f_y}} \text{ (for ANSI/AISC 360-16)} \tag{17}$$

$$b/t \le 2.01 \times \frac{260}{\sqrt{f_y}} \text{ (for ASCE/SEI 48-11)} \tag{18}$$

$$\lambda_p \le 0.653 \text{ (for DSM)} \tag{19}$$

4.2.1 Cross-sectional capacity

The current ASCE/SEI 48-11 and DSM design methods on the cross-sectional capacities of OctHSs were evaluated. The design methods specified in EN 1993-1-5 and ANSI/AISC 360-16 were also assessed to examine the feasibility to extend these methods to the design of OctHSs. The ultimate load (N_u) obtained from test and FE results was compared with the predicted capacities ($N_{u,pred}$) determined in accordance with ASCE/SEI 48-11, DSM, EN 1993 and ANSI/AISC 360-16. All partial factors were set to unity to allow for direct comparisons. Fig. 16 shows $N_u/N_{u,pred}$ ratios of OctHs stub columns. Table 6 summarises the results of statistical analyses of $N_u/N_{u,pred}$ ratios. The mean values of $N_u/N_{u,pred}$ for all OctHSs obtained from ASCE/SEI 48-11, DSM, EN 1993-1-5 and ANSI/AISC 360-16 are 0.98, 1.00, 1.00 and 1.03 with corresponding COVs of 0.09, 0.06, 0.07 and 0.07. All the design methods underestimate the cross-sectional capacities for Class 1-3 or non-slender sections as a result of strain-hardening, giving the mean $N_u/N_{u,pred}$ values of 1.06, 1.06, 1.06 and 1.10, respectively. However, the design methods tend to overestimate the capacities for Class 4 or slender sections. The mean $N_u/N_{u,pred}$ values for slender OctHSs obtained from ASCE/SEI 48-11, DSM, EN 1993-1-5 and ANSI/AISC 360-16 are 0.92, 0.96, 0.95 and 0.98 with corresponding COVs of 0.06, 0.04, 0.03 and 0.04. It is shown that the strength predictions for slender sections from ASCE/SEI 48-11 are slightly unsafe, and ANSI/AISC 360-16 produces relatively satisfactory capacity predictions when compared with test and FE results.

5. Conclusions

This paper has presented an experimental and numerical investigation into the stub column behaviours of cold-formed octagonal hollow sections (OctHSs). A total of 16 OctHS stub column tests were conducted. Tensile coupons were extracted from both flat and corner portions of hollow sections to determine corresponding material properties. Finite element (FE) models were developed using commercially available software ABAQUS to replicate the test results generated in this study. Residual stresses were found to have negligible effect on the stub column behaviours in terms of ultimate load and axial load-end shortening curves. The degree to which the enhanced corner material properties should be extended in OctHSs was investigated as well. It was found that FE models with the corner material properties extended to a width of material thickness *t* beyond the curved portions offer the best agreement with test results. The validated FE models were then adopted to conduct parametric studies to supplement the test database.

The cross-section slenderness limits specified in current design methods, EN 1993-1-1, ANSI/AISC 360-16, ASCE/SEI 48-11 and DSM were evaluated against the test results in conjunction with the FE results. It was found that current limits are not safe for the design of OctHSs. New cross-sectional slenderness limits in accordance with EN 1993-1-1, ANSI/AISC 360-16, ASCE/SEI 48-11 and DSM were then proposed based on the test and FE results. The cross-sectional capacity predictions obtained from EN 1993-1-1, ANSI/AISC 360-16, ASCE/SEI 48-11 and DSM were compared with test and FE results. It is shown that the strength predictions for slender sections from ASCE/SEI 48-11 are slightly unsafe, while ANSI/AISC 360-16 produces relatively satisfactory capacity predictions when compared with test and FE results. All the design methods tend to overestimate the capacities for Class 4 or slender sections. Further investigations into more effective design of octagonal hollow sections are currently under way.

Acknowledgement

The research work presented in this paper was supported by a grant from the Research Grants Council of the Hong Kong Special Administrative Region, China (Project no. PolyU 152492/16E). The authors also appreciate the support from the Chinese National Engineering Research Centre for Steel Construction (Hong Kong Branch) at The Hong Kong Polytechnic University. The authors would also like to thank the technical staff, Mr. K.H. Wong, Mr. Y.H. Yiu and Mr. M.C. Ng, of the Structural Engineering Research Laboratory at The Hong Kong Polytechnic University for their assistance on the experimental works.

Reference

[1] J.L. Ma, T.M. Chan, B. Young, Material properties and residual stresses of cold-formed high strength steel hollow sections, J Construct Steel Res 109 (2015) 152-165.
[2] Wardenier J. “Hollow sections in structural applications”, 2nd ed. Geneva: CIDECT; 2011.
[3] J. Wang, S. Afshan, N. Schillo, M. Theofanous, M. Feldmann, L. Gardner, Material properties and compressive local buckling response of high strength steel square and rectangular hollow sections, Eng Struct 130 (2017) 297-315.
[4] J.L. Ma, T.M. Chan, B. Young, Experimental investigation on stub-column behavior of cold-formed high-strength steel tubular sections, J Struct Eng, 142(5) (2016) 04015174.
[5] X. Lan, J. Chen, T.M. Chan, B. Young, The continuous strength method for the design of high strength steel tubular sections in compression, Eng Struct 162 (2018) 177-187.

[6] J.L. Ma, T.M. Chan, B. Young, Experimental investigation of cold-formed high strength steel tubular beams, Eng Struct, 126, (2016) 200-209.
[7] X. Lan, J. Chen, T.M. Chan, B. Young, The continuous strength method for the design of high strength steel tubular sections in bending, J Constr Steel Res 160 (2019) 499-509.
[8] H. Fang, T.M. Chan, B. Young, Structural performance of cold-formed high strength steel tubular columns, Eng Struct, 177 (2018) 473-488.
[9] R.M. Slocum, Considerations in the design and fabrication of tubular steel transmission structures. Proceedings of the fifteenth international symposium on tubular structures – ISTS 15, 27–29 May 2015, Rio de Janeiro, Brazil. 2015.
[10] H. Fang, T.M. Chan, B. Young, Material properties and residual stresses of octagonal high strength steel hollow sections, J Construct Steel Res, 184 (2018) 479-490.
[11] J. Chen, H. Liu, T.M. Chan, Material properties and residual stresses of cold-formed octagonal hollow sections, J Construct Steel Res, https://doi.org/10.1016/j.jcsr.2020.106078.
[12] ASCE/SEI 48-11. Design of steel transmission pole structures, Reston, Virginia, American Society of Civil Engineers, 2011.
[13] EN 1993-1-1. Eurocode 3: Design of steel structures – Part 1.1: General rules and rules for buildings, Brussels, European Committee for Standardization (CEN); 2005.
[14] EN 1993-1-12. Eurocode 3: Design of steel structures-Part 1-12: additional rules for the extension of EN 1993 up to steel grades S700, Brussels, European Committee for Standardization (CEN); 2007.
[15] ANSI/AISC 360-16. Specification for structural steel buildings. Chicago, American Institute of Steel Construction (AISC); 2016.
[16] J.Y. Zhu, T.M. Chan, B. Young, Cross-sectional capacity of octagonal tubular steel stub columns under uniaxial compression, Eng Struct, 184 (2019) 480-494.
[17] Aoki T, Migita Y, Fukumoto Y. Local buckling strength of closed polygon folded section columns. J Constr Steel Res 1991;20(4):259–70.
[18] Y. Migita, T. Aoki, Y. Fukumoto, Local and interaction buckling of polygonal section steel columns, J. Struct. Eng. 118 (1992) 2659–2676.
[19] Migita Y, Fukumoto Y. Local buckling behaviour of polygonal sections. J Constr Steel Res 1997 Feb 1;41(2–3):221–33.
[20] Godat A, Legeron F, Bazonga D. Stability investigation of local buckling behavior of tubular polygon columns under concentric compression. Thin-Walled Struct 2012;1(53):131–40.
[21] Zhu JY, Chan TM. Behaviour of polygonal-shaped steel-tube columns filled with high-strength concrete. Proc Inst Civil Eng – Struct Build 2018;171(2):96–112.
[22] H. Fang, T.M. Chan, B. Young, Behavior of octagonal high strength steel tubular stub columns, J. Struct. Eng. (ASCE), 2019, 145(12): 04019150
[23] EN ISO 6892-1:2016, Metallic materials– tensile testing. Part 1: Method of test at ambient temperature, Brussels, European Committee for Standardization (CEN); 2016.
[24] Y. Huang, B. Young, The art of coupon tests, J Constr Steel Res 96 (2014) 159–175.

[25] K. Karren, Corner properties of cold-formed steel shapes. J. Struct. Div. (ASCE), (1967) 93:401-32.
[26] Gardner L, Nethercot D.A., Experiments on stainless steel hollow sections—Part 1: Material and cross-sectional behaviour, J Constr Steel Res 60 (2004) 1291–1318.
[27] ABAQUS/Standard. Version 6.13-1. USA: K. a. S. Hibbit; 2013.
[28] Gardner L, Nethercot D.A., Numerical modelling of stainless steel structural components-a consistent approach, J Struct Eng (ASCE), 130(10) 2004 1586-1601.
[29] AISI S100. North American specification for the design of cold-formed steel structural members, Washington: American Iron and Steel Institute (AISI); 2016.
[30] J.G. Teng, S.T. Smith, L.Y. Ngok. Local buckling of thin-walled polygonal columns subjected to axial compression or bending. Adv. Steel Struct. 1999, 109-115.
[31] EN 1993-1-5. Eurocode 3: Design of steel structures – Part 1.5: Plated structural elements. Brussels: European Committee for Standardization (CEN); 2006.

Table 1. Measured cross-sectional dimensions of OctHS specimens.

Specimen	H mm	B mm	t mm	L mm	r_o mm	r_i mm	b mm	b/t -	A mm^2	ω_0 mm
O60×3-CF1	147.5	61.1	3.03	431	10.0	7.0	52.8	17.4	1440	0.19
O60×3-CF1#	147.1	60.9	3.05	432	9.5	7.0	53.0	17.4	1424	0.18
O60×3-CF2	146.8	60.8	3.04	434	10.0	7.0	52.5	17.3	1437	0.20
O60×3-CF2#	147.4	61.0	3.05	433	10.0	7.5	52.8	17.3	1425	0.23
O75×3-CF1	184.8	76.6	3.05	543	10.5	7.5	67.9	22.2	1825	0.20
O75×3-CF1#	184.8	76.6	3.04	542	10.0	7.0	68.3	22.5	1821	0.27
O75×3-CF2	184.4	76.4	3.05	544	10.0	7.0	68.1	22.3	1821	0.16
O75×6-CF1	183.5	76.0	5.83	543	19.0	13.5	60.3	10.3	3372	0.46
O75×6-CF1#	184.7	76.5	5.83	544	18.5	12.5	61.2	10.5	3438	0.48
O75×6-CF2	184.1	76.3	5.83	542	19.0	13.5	60.5	10.4	3384	0.39
O90×3-CF1	222.0	92.0	3.05	641	10.0	7.5	83.7	27.4	2179	0.14
O90×3-CF2	220.3	91.3	3.05	645	10.0	7.0	83.0	27.2	2185	0.21
O90×3-CF2#	220.4	91.3	3.06	647	10.5	7.5	82.6	27.0	2191	0.17
O105×3-CF1	257.8	106.8	3.05	756	10.0	7.0	98.5	32.3	2564	0.39
O105×3-CF1#	256.5	106.2	3.05	755	10.0	7.0	98.0	32.1	2550	0.27
O105×3-CF2	255.9	106.0	3.04	757	10.0	7.5	97.7	32.1	2514	0.24

Note: # indicates a repeated test.

Table 2. Measured material properties of parent metals.

Steel	E_s GPa	v	f_y MPa	f_u MPa	ε_{sh} %	ε_u %	ε_f %
3 mm	209.5	0.28	546.5	625.8	2.2	10.9	26.0
6 mm	213.3	0.28	580.7	666.1	2.3	10.1	25.4

Table 3. Mean material properties of OctHS flat coupons.

Steel	$E_{s,f}$ GPa	$f_{y,f}$ MPa	$f_{u,f}$ MPa	$\varepsilon_{u,f}$ %	$\varepsilon_{f,f}$ %
3 mm	209.8	540.8	622.7	10.8	27.8
6 mm	213.9	581.0	669.1	11.7	28.1

Table 4. Mean material properties of OctHS corner coupons.

Steel	$E_{s,c}$ GPa	$f_{y,c}$ MPa	$f_{u,c}$ MPa	$\varepsilon_{u,c}$ %	$\varepsilon_{f,c}$ %
3 mm	201.1	655.1	689.9	1.24	15.9
6 mm	198.2	735.0	775.9	1.33	14.4

Table 5. Test results of OctHS stub column tests.

Specimen	N_u kN	δ_u mm	N_y kN	N_u/N_y	FE N_u / Test N_u			
					w/o corner properties	No extension	Extended to t	Extended to $2t$
O60×3-CF1	822	1.95	797	1.03	0.96	0.98	1.00	1.03
O60×3-CF1#	831	1.96	785	1.06	0.95	0.98	1.00	1.02
O60×3-CF2	830	2.06	796	1.04	0.95	0.97	0.99	1.02
O60×3-CF2#	839	2.03	786	1.07	0.94	0.96	0.98	1.01
O75×3-CF1	1031	2.28	1007	1.02	0.96	0.97	0.99	1.00
O75×3-CF1#	1019	2.06	1003	1.02	0.96	0.97	0.99	1.00
O75×3-CF2	1030	2.33	1003	1.03	0.96	0.98	0.99	1.01
O75×6-CF1	2132	8.32	2046	1.04	0.97	1.02	1.04	1.07
O75×6-CF1#	2141	8.57	2087	1.03	0.98	1.03	1.06	1.08
O75×6-CF2	2153	8.85	2053	1.05	0.96	1.01	1.03	1.04
O90×3-CF1	1180	2.02	1194	0.99	0.98	0.99	1.00	1.00
O90×3-CF2	1181	2.43	1200	0.98	0.96	0.97	0.97	0.98
O90×3-CF2#	1230	2.26	1205	1.02	0.94	0.94	0.95	0.96
O105×3-CF1	1160	2.12	1405	0.83	1.00	1.00	1.00	1.01
O105×3-CF1#	1191	2.07	1398	0.85	1.00	1.00	1.00	1.01
O105×3-CF2	1207	2.13	1375	0.88	0.99	0.99	0.99	1.00
Mean					0.97	0.99	1.00	1.01
CoV					0.02	0.02	0.02	0.03

Note: # indicates a repeated test.

Table 2. Statistical analysis of OctHS stub columns.

	$N_u / N_{u,ASCE}$			$N_u / N_{u,DSM}$			$N_u / N_{u,EC3}$			$N_u / N_{u,AISC}$		
	Non-slender	Slender	All	Non-slender	Slender	All	Non-slender	Slender	All	Non-slender	Slender	All
Mean	1.06	0.92	0.98	1.06	0.96	1.00	1.06	0.95	1.00	1.10	0.98	1.03
CoV	0.04	0.06	0.09	0.04	0.04	0.06	0.04	0.03	0.07	0.05	0.04	0.07

Fig. 1. Octagonal section lighting column (New York, US).

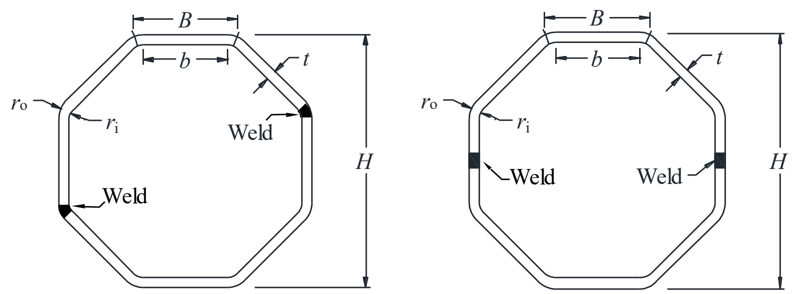

(a) CF1 (b) CF2

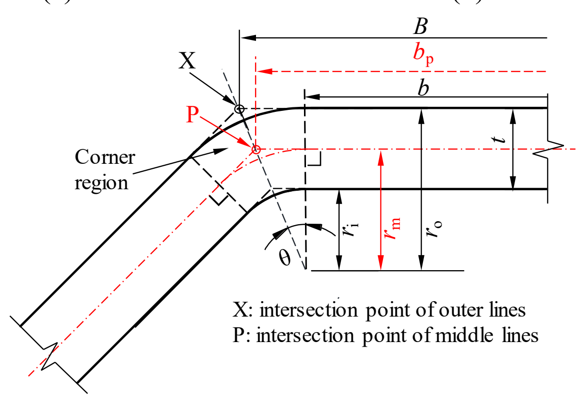

(c) Corner portion

Fig. 2. Fabrication routes and definition of symbols for OctHSs.

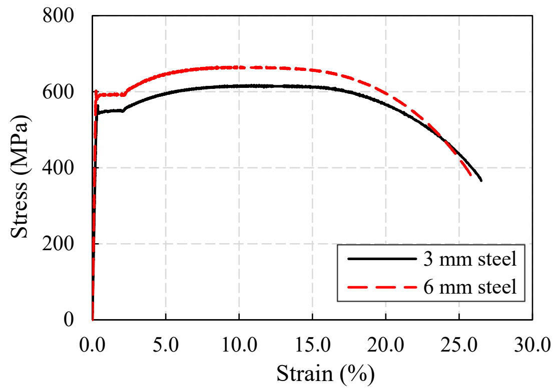

Fig. 3. Typical stress-strain curves of tensile coupon tests.

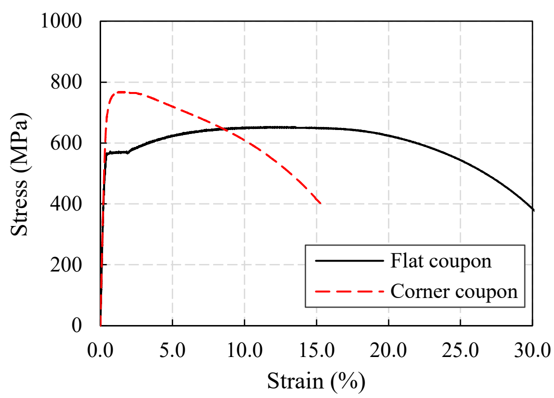

Fig. 4. Typical stress-strain curves of flat and corner coupons.

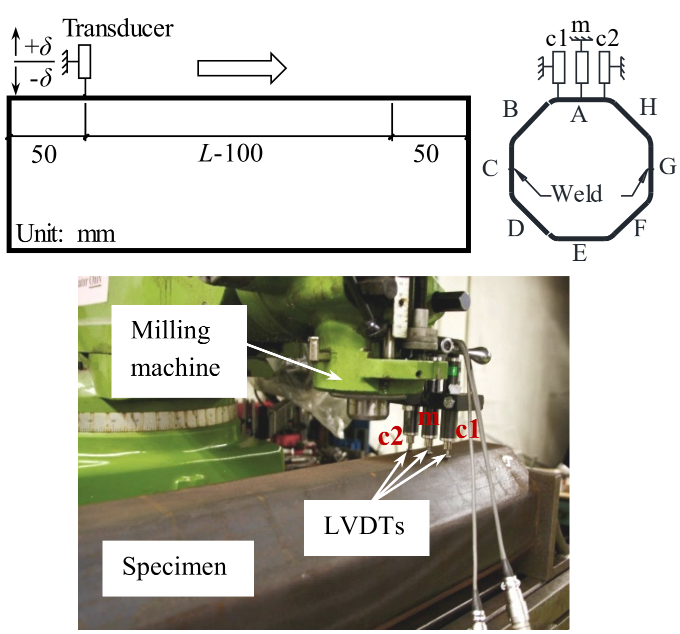

Fig. 5. Arrangement of geometric imperfection measurement.

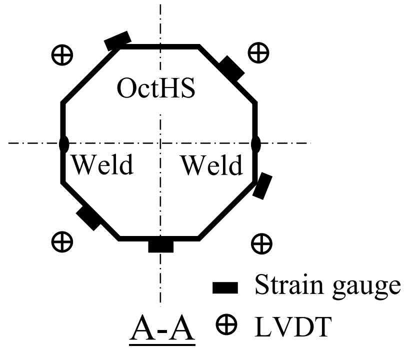

(a) Strain gauge and LVDT arrangements

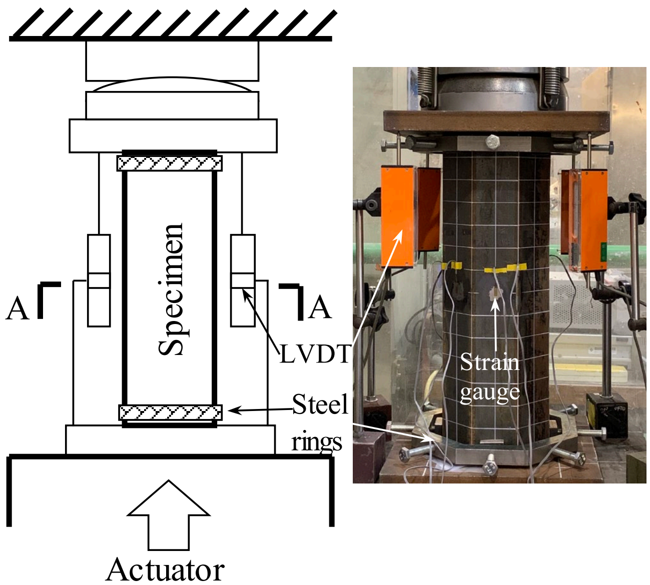

(b) Schematic and experimental views of test arrangements

Fig. 6. Test arrangements for stub column tests.

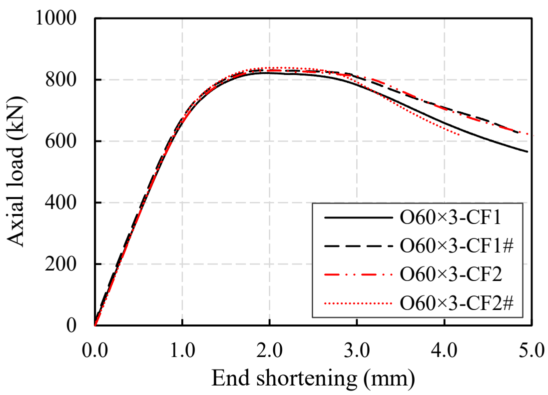

(a) O60×3

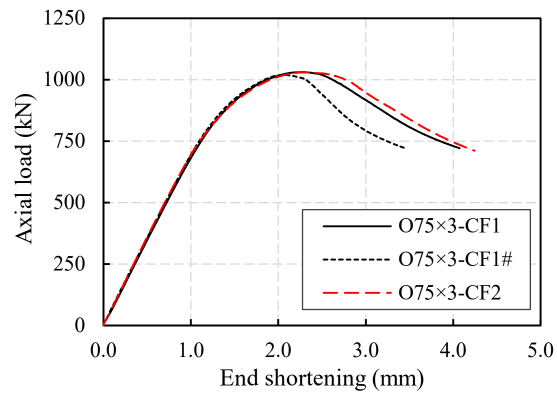

(b) O75×3

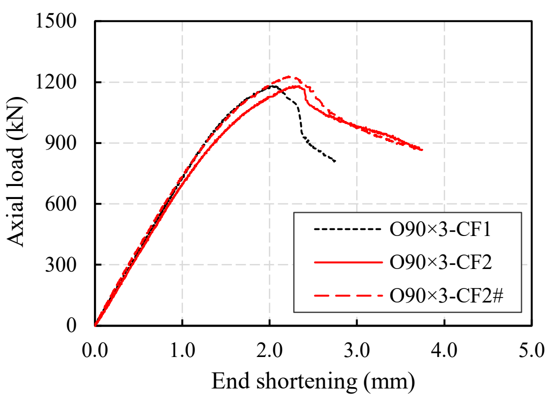

(c) O90×3

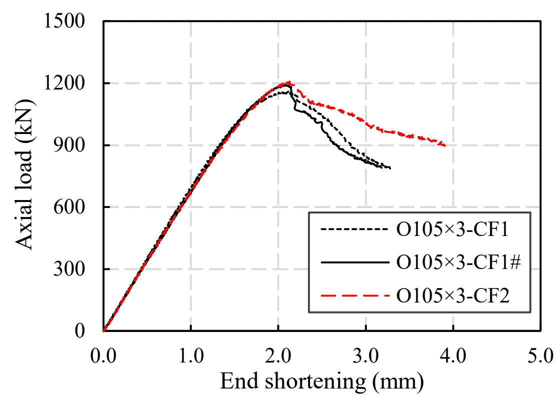

(d) O105×3

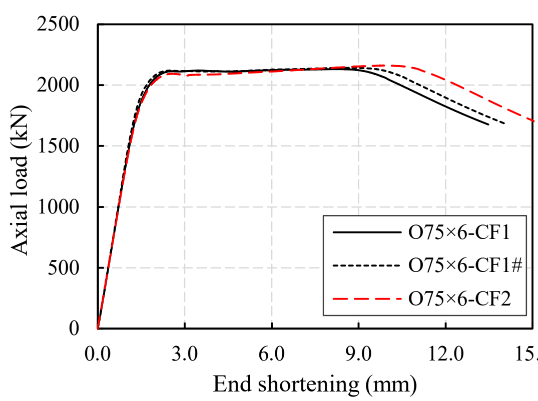

(e) O75×6

Fig. 7. Axial load versus end shortening curves of OctHS tests.

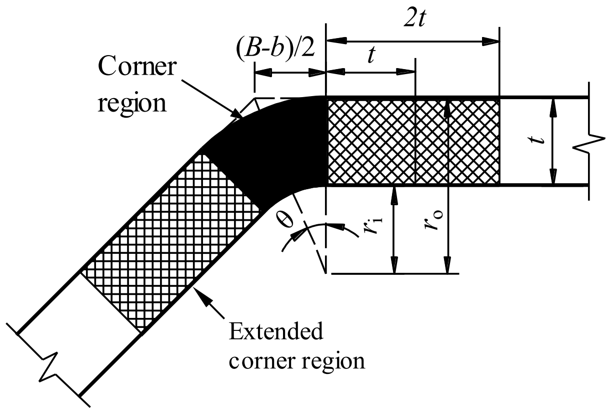

Fig. 8. Extents of corner regions in FE.

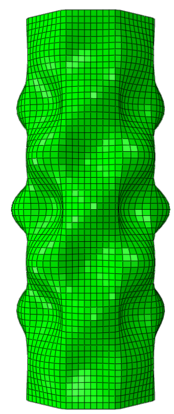

Fig. 9. Lowest eigenmodes of OctHS stub column.

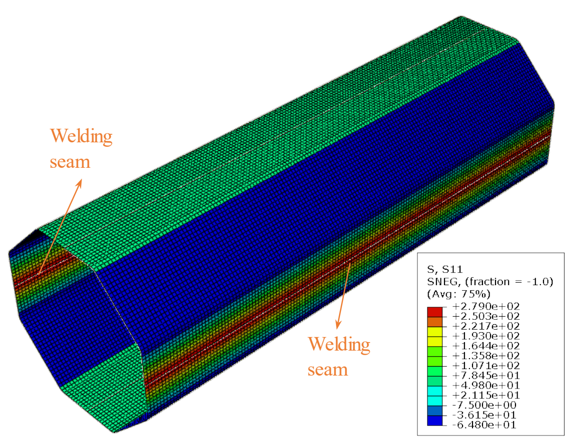

Fig. 10. Typical residual stress distribution in modelled O75×3-CF2 (in MPa).

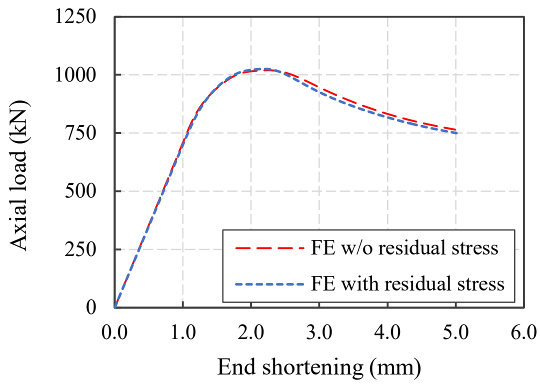

Fig. 11. Effect of residual stresses on specimen O75×3-CF2.

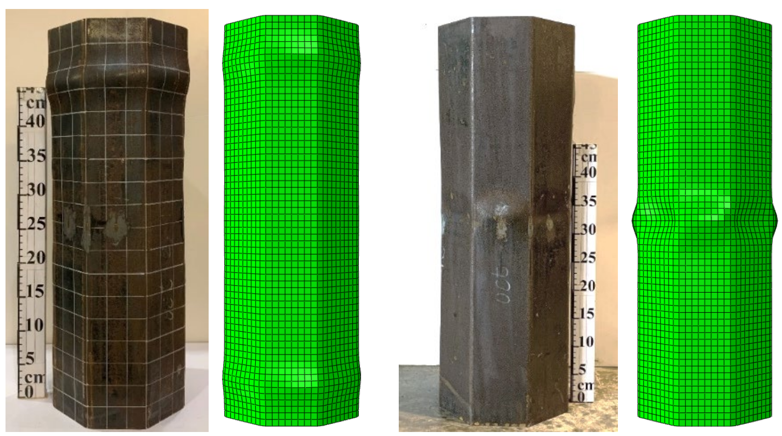

(a) O75×6-CF2 (b) O90×3-CF1

Fig. 12. Typical failure modes from stub column tests and corresponding FE models.

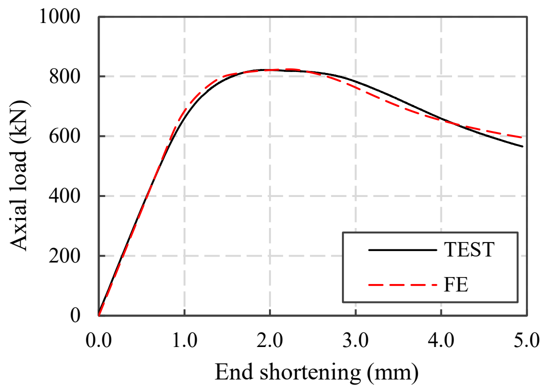

(a) O60×3-CF1 (Corner properties extended to *t*)

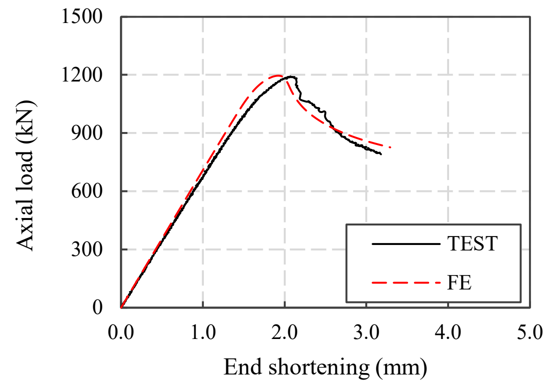

(b) O105×3-CF1# (Corner properties extended to *t*)

Fig. 13. Typical axial load versus end shortening curves from tests and corresponding FE models.

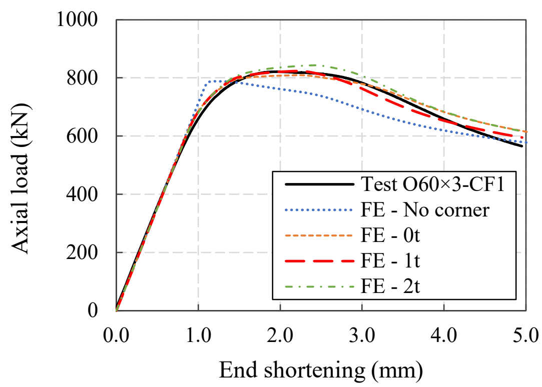

Fig. 14. Effect of the extension of corner material properties.

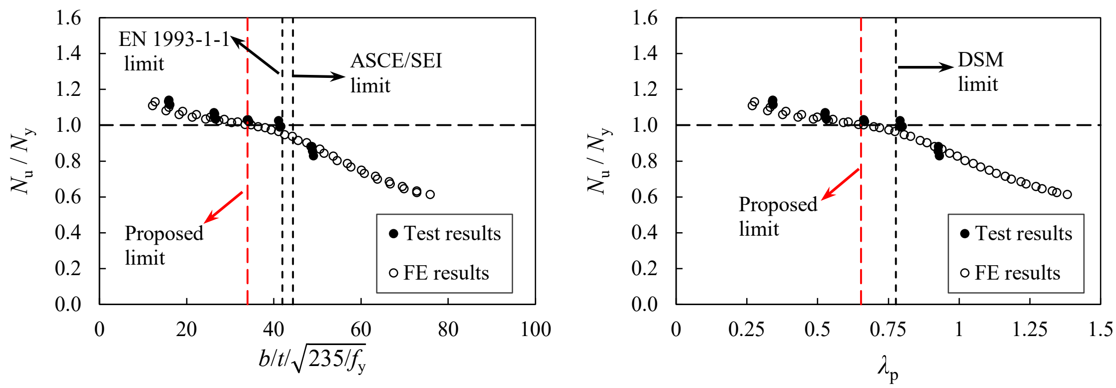

Fig. 15. Assessment on cross-section slenderness limits.

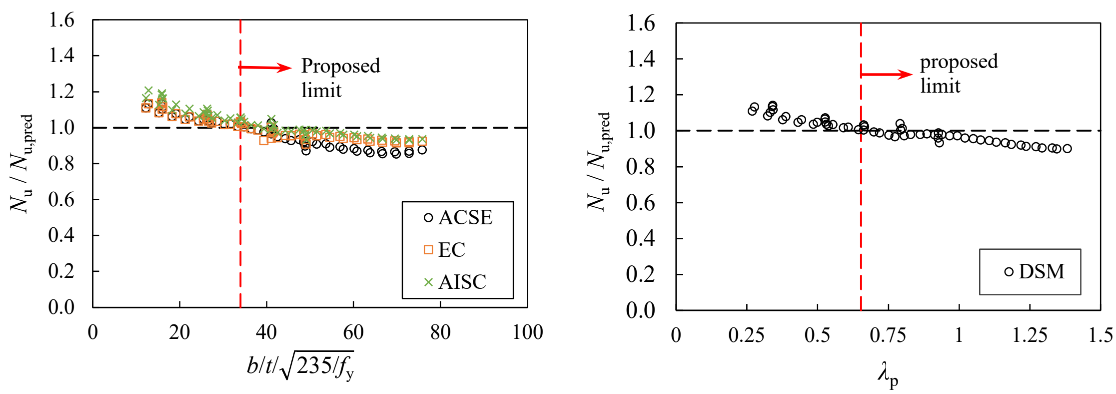

Fig. 16. Assessment on cross-sectional capacities.